In particular, lower animals with few photoreceptor cells—and therefore very limited visual fields—use scanning to detect objects and to learn or recognize landmarks beyond their visual field coverage[21,22]. In humans, scanning local information with the fovea during surface integration also ensures that the information sampled has better spatial resolution than that afforded by the peripheral retina[22]. □

Methods

Observers

Ten naive observers with self-reported normal vision and informed consent participated in the various experiments. All performed the experiments with their motor dominant, right eye. To limit the monocular field of view to a preselected size, a pair of clear safety goggles was painted black all over except for a rectangular area (aperture) in front of the right eye with the appropriate field extent. For all aperture sizes used, the observers were unable to see their body and feet without rotating their heads. The goggles were worn throughout the experiments except during the full-view (control) condition, in which the observers wore an opaque patch over the left eye without the goggles. They were not given any feedback about their performances.

Judging absolute distance by using the blind-walking task

The observer previewed an orange–red disk target (7.62 cm in diameter and 2.54 cm high) on a flat grass surface and judged its absolute distance. Then he pulled a blindfold over his eyes (goggles) and walked forward to traverse the remembered target distance. He stopped upon reaching the remembered target location and remained there to allow the experimenter to measure the walked distance. Thereafter, the experimenter led the observer, still in blindfold, back to the starting point to ready for a new trial. Four target distances (4, 5, 6 and 7 m) were tested in a randomized order. Each distance was tested twice and the average was taken as the final result.

Judging relative length-in-depth by using a perceptual matching task

Two white pipes, 3 cm in diameter, were used to construct the L-shaped target. The frontoparallel arm (W) of the L-shaped target was fixed at 40.5 cm, and the length of the arm in depth (Z) was adjustable. During a trial, the observer kept his head still and judged whether the width of arm-Z was equal to the length of arm-W. If not, the observer pulled a blindfold over his eyes (goggles) and instructed the experimenter to adjust the length of arm-Z. After the experimenter finished making the adjustment and had walked away from the L-shaped target, the observer was told to remove the blindfold and to compare the width and length of the L-shaped target again. This was repeated several times until the observer was satisfied that the two arms matched in width and length. The base of the L-shaped target to the observer defined the viewing distance, which was one of three distances (5, 6 and 7 m) that was measured in a randomized order. Each distance was tested twice and the average was taken as the final result.

Judging distance in the dark

The test target, a 0.23° internally illuminated red table tennis ball, was placed at one of four distances (2.50, 3.75, 5.00 and 6.25 m) either on the floor or 0.5 m above it. Trials with targets above the floor served as catch trials (one-third of the total trials). Other than the test target, the room was completely dark so that the observer could not access other visual cues. For each trial, the observer ($n = 9$) previewed the distance and height of the target with the dominant eye. After this, the target was extinguished and the observer walked blindly to the remembered target location. Upon reaching his destination, the observer gestured the perceived height of the remembered target with his hand. The walked distance and gestured height are taken as the judged distance and height of the target, respectively. This procedure was used for all three conditions tested (free head motion, near-to-far head motion and far-to-near head motion).

Data analysis

We applied the two-way analysis of variance with repeated-measures analysis to our data to obtain the F and P values indicated in the text. Following convention, the main effect and interaction are presented in order.

Received 12 August 2003; accepted 20 January 2004; doi:10.1038/nature02350.

1. Gogel, W. C. & Tietz, J. D. A comparison of oculomotor and motion parallax cues of egocentric distance. *Vision Res.* **19,** 1161–1170 (1979).
2. Philbeck, J. W. & Loomis, J. M. Comparison of two indicators of perceived egocentric distance under full-cue and reduced-cue conditions. *J. Exp. Psychol. Hum. Percept. Perform.* **23,** 72–85 (1997).
3. Ooi, T. L., Wu, B. & He, Z. J. Distance determined by the angular declination below the horizon. *Nature* **414,** 197–200 (2001).
4. Thomson, J. A. Is continuous visual monitoring necessary in visually guided locomotion? *J. Exp. Psychol. Hum. Percept. Perform.* **9,** 427–443 (1983).
5. Rieser, J. J., Ashmead, D., Talor, C. & Youngquist, G. Visual perception and the guidance of locomotion without vision to previously seen targets. *Perception* **19,** 675–689 (1990).
6. Loomis, J., DaSilva, J., Fujita, N. & Fukusima, S. Visual space perception and visually directed action. *J. Exp. Psychol.* **18,** 906–921 (1992).
7. Loomis, J., DaSilva, J., Philbeck, J. W. & Fukusima, S. Visual perception of location and distance. *Curr. Dir. Psychol. Sci.* **5,** 72–77 (1996).
8. Sinai, M. J., Ooi, T. L. & He, Z. J. Terrain influences the accurate judgement of distance. *Nature* **395,** 497–500 (1998).
9. Loomis, J. M. & Knapp, J. M. in *Virtual and Adaptive Environments* (eds Hettinger, L. J. & Hass, M. W.) 21–46 (Erlbaum, Hillsdale, New Jersey, 2003).
10. Hagen, M. A., Jones, R. K. & Reed, E. S. On a neglected variable in theories of pictorial perception: Truncation of the visual field. *Percept. Psychophys.* **23,** 326–330 (1978).
11. Dolezal, H. *Living in a World Transformed: Perceptual and Performatory Adaptation to Visual Distortion* (Academic, New York, 1982).
12. Loomis, J. M. & Philbeck, J. W. Is the anisotropy of perceived 3-D shape invariant across scale? *Percept. Psychophys.* **61,** 397–402 (1999).
13. Loomis, J. M., Philbeck, J. W. & Zahorik, P. Dissociation of location and shape in visual space. *J. Exp. Psychol. Hum. Percept. Perform.* **28,** 1202–1212 (2002).
14. Gibson, J. J. *The Perception of the Visual World* (Houghton, Mifflin, Boston, Massachusetts, 1950).
15. Gibson, J. J. The perception of visual surfaces. *Am. J. Psychol.* **63,** 367–384 (1950).
16. Freeman, R. B. Jr Effect of size on visual slant. *Psychol. Rev.* **72,** 501–504 (1956).
17. Braunstein, M. L. Motion and texture as sources of slant information. *J. Exp. Psychol.* **78,** 247–253 (1968).
18. Gibson, J. J. & Cornsweet, J. The perceived slant of visual surfaces—optical and geographical. *J. Exp. Psychol.* **44,** 11–15 (1952).
19. Sedgwick, H. A. in *Handbook of Perception and Human Performance* (eds Boff, K. R., Kaufman, L. & Thomas, J. P.) 21.1–21.57 (Willey, New York, 1986).
20. Meng, J. C. & Sedgwick, H. A. Distance perception mediated through nested contact relations among surface. *Percept. Psychophys.* **63,** 1–15 (2001).
21. Land, M. F. Scanning eye movements in a heteropod mollusc. *J. Exp. Biol.* **96,** 427–430 (1982).
22. Land, M. F. Motion and vision: why animals move their eyes. *J. Comp. Physiol. A* **185,** 341–352 (1999).

Acknowledgements This research was supported in part by a grant from NIH to Z.J.H. and T.L.O. and by a RIG grant from the University of Louisville to Z.J.H.

Competing interests statement The authors declare that they have no competing financial interests.

Correspondence and requests for materials should be addressed to Z.J.H. (zjhe@louisville.edu) or T.L.O. (tlooi@pco.edu).

Inactivation of *hCDC4* can cause chromosomal instability

Harith Rajagopalan[1], Prasad V. Jallepalli[1,2], Carlo Rago[1], Victor E. Velculescu[1], Kenneth W. Kinzler[1], Bert Vogelstein[1,3] & Christoph Lengauer[1]

[1]*The Sidney Kimmel Comprehensive Cancer Center, Johns Hopkins University School of Medicine, Baltimore, Maryland 21231, USA*
[2]*Molecular Biology Program, Memorial Sloan-Kettering Cancer Center, New York, New York 10021, USA*
[3]*Howard Hughes Medical Institute, The Johns Hopkins University Medical Institutions, Baltimore, Maryland 21231, USA*

Aneuploidy, an abnormal chromosome number, has been recognized as a hallmark of human cancer for nearly a century[1]; however, the mechanisms responsible for this abnormality have remained elusive. Here we report the identification of mutations in *hCDC4* (also known as *Fbw7* or *Archipelago*) in both human colorectal cancers and their precursor lesions. We show that genetic inactivation of *hCDC4*, by means of targeted disruption of the gene in karyotypically stable colorectal cancer cells, results in a striking phenotype associated with micronuclei and chromosomal instability. This phenotype can be traced to a defect in the execution of metaphase and subsequent transmission of chromosomes, and is dependent on cyclin E—a protein that is regulated by hCDC4 (refs 2–4). Our data suggest that chromosomal instability is caused by specific genetic alterations in a large fraction of human cancers and can occur before malignant conversion.

CDC4 is an evolutionarily conserved E3 ubiquitin ligase that is thought to be involved in regulating the G1–S cell-cycle checkpoint by targeting proteins for destruction by the SCF complex of proteins[2]. Mutations in the *hCDC4* gene were originally identified in a few breast and ovarian cancer cell lines and have been subsequently found in endometrial cancers[5–7]. Here we have

addressed the role that *hCDC4* may have in colorectal tumorigenesis through mutational analysis and genetic dissection.

To determine whether *hCDC4* is genetically altered, its coding exons were amplified by polymerase chain reaction (PCR) from 190 colorectal tumours and sequenced. Somatic mutations in the *hCDC4* gene were found in 22 of the 190 samples. Nonsense mutations at codons 224, 278, 303, 393 and 446 were found in eight tumours. All of these mutations are predicted to result in truncation of the protein at a position amino-terminal to the fourth WD40 domain, thereby interrupting the binding of hCDC4 to its substrate (Fig. 1a). Six of the tumours had biallelic inactivations, either because of allelic loss of the wild-type gene (in three tumours) or because of two independent point mutations on opposite alleles (Supplementary Table 1). The 22 cancers with *hCDC4* mutations represent all stages of colorectal cancer. To determine the point in tumorigenesis at which the mutations occur, we sequenced *hCDC4* in adenomas—benign tumours that are the precursors of cancers. Out of 58 colorectal adenomas tested, four mutations were identified (Fig. 1a and Supplementary Table 1). Notably, two of these mutations occurred in adenomas less than 1 cm in diameter; such lesions have been shown to progress to malignancy only after 10–20 yr.

If the numerous missense changes in *hCDC4* inactivate the protein product, one would expect the mutations to cluster in key functional domains of the hCDC4 protein. Crystal structure coordinates of yeast CDC4 bound to a phosphopeptide of human cyclin E were used to reconstruct the spatial relationship between the two proteins[8,9]. All but one of the missense mutations occurred in the WD40 domain repeats in the 3′ region of the gene, and many resulted in the elimination of specific arginines that are thought to be involved in substrate-binding specificity[8,10]. Notably, 18 of the 19 missense changes occurred at the surface of the eight-bladed β-propeller structure produced by the WD40 repeats (Fig. 1c, d). The lone remaining missense mutation occurred in the region encoding the F-box and may disrupt the binding of hCDC4 to the remainder of the SCF complex. Co-immunoprecipitation experiments also showed that cyclin E bound better to wild-type hCDC4 than to a mutationally altered protein (Fig. 1b), thus corroborating the suggestions from the structural data.

The several mutations identified above provide compelling evidence that *hCDC4* is involved in colorectal tumorigenesis. But how? Some studies have suggested that hCDC4 controls cell proliferation by regulating replication, whereas others have proposed that hCDC4 may have a role in genetic instability[6,11–13]. To determine the consequences of *hCDC4* inactivation in colorectal tumorigenesis, we used homologous recombination to disrupt both alleles of *hCDC4* in HCT116, a karyotypically stable colorectal carcinoma cell line (ref. 14 and Fig. 2a). Successful targeting was confirmed by PCR-based analysis of DNA and RNA (Fig. 2b, c). Two clones were obtained, each of which behaved identically in the assays described below.

The absence of *hCDC4* resulted in a high increase in cyclin E (Fig. 2d), indicating functional conservation of the hCDC4/cyclin E pathway originally identified in yeast and insect cells[6,7]. The growth of *hCDC4*$^{-/-}$ cells was indistinguishable from that of parental cells, and no obvious differences were observed in plating efficiency, cell-cycle profile or saturation density (data not shown); however, microscopic examination revealed several marked cytological abnormalities. First, *hCDC4*-deficient cells showed nuclear atypia characterized by micronuclei and lobulated or elongated nuclei, none of which was observed in parental wild-type cells (18.3% versus 1.0%, $P < 10^{-5}$, $n = 400$ cells for each cell type; Fig. 3a–d). The fraction of cells with such aberrant nuclei did not vary with the generational age of the cells, as such cells were found in both early and late passage cultures (Supplementary Table 2 and data not shown).

Second, immunofluorescence staining showed an increase in the frequency of multipolar spindles in *hCDC4*$^{-/-}$ cells (Fig. 3e, f), a mitotic defect that was rarely observed in wild-type cells (7% versus 0.5%; $P < 0.001$). Fluorescence *in situ* hybridization (FISH) of a pan-centromeric probe to interphase nuclei showed that a few micronuclei had one or two signals, but most micronucleated chromosomal material lacked detectable centromeric DNA (Fig. 3c). Notably, none of the *hCDC4*$^{-/-}$ knockout clones showed an increase in apoptosis (data not shown), indicating that the generation of micronuclei was not likely to be fatal in cellular replication.

To elucidate the basis of these cellular abnormalities, we used time-lapse videomicroscopy of *hCDC4*$^{-/-}$ and parental cells to visualize chromosomes in living cells[15]. Eight of twenty-six (31%) mitoses in *hCDC4*$^{-/-}$ cells did not execute chromosome congression during metaphase ($P < 0.002$; Supplementary Fig. 1 and

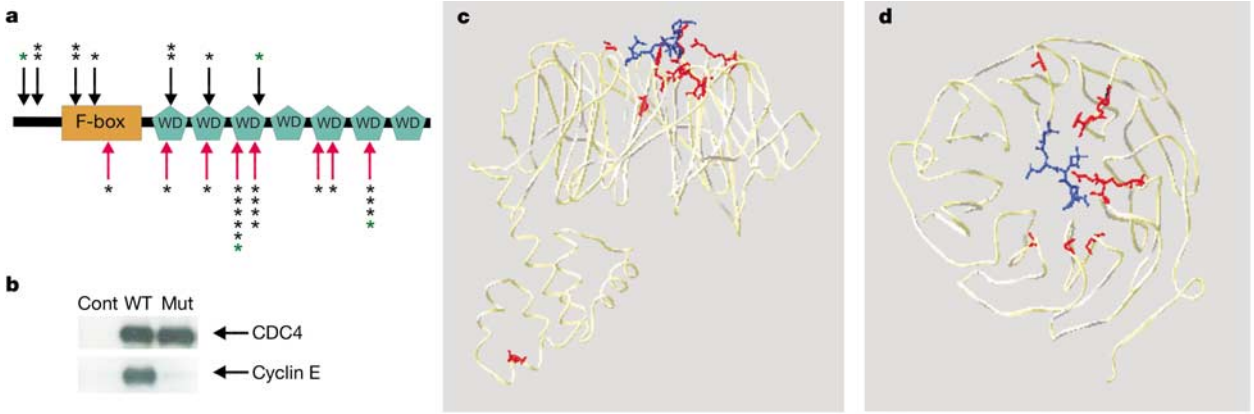

Figure 1 *hCDC4* mutations in colorectal cancers and adenomas. **a**, Location (arrows) and frequency (asterisks) of mutations in *hCDC4*. Black arrows indicate nonsense mutations, red arrows indicate missense mutations, black asterisks indicate the number of mutations found in cancers, green asterisks show mutations found in adenomas. **b**, Western blotting for Myc (Myc-tagged CDC4) and cyclin E after immunoprecipitation with an antibody against Myc. Cont, untransfected cells; WT, cells co-transfected with cyclin E and Myc-tagged wild-type CDC4; Mut, cells co-transfected with cyclin E and Myc-tagged mutant CDC4 (Arg465Cys). **c**, **d**, Three-dimensional views of yeast CDC4 bound to human cyclin E[8,9]. CDC4 is shown in yellow, cyclin E in blue. Amino acids in CDC4 that align with residues affected by missense mutations in hCDC4 are labelled in red. **c**, Longitudinal view. **d**, View down the *z*-axis.

Supplementary Movie). The full chromosome complement did not align on the metaphase plate despite numerous 'attempts', and mitosis ultimately proceeded with an unequal segregation of DNA content. In two cells, the formation of a micronucleus was observed during filming. The duration of mitosis was extremely prolonged in all cells, lasting 147 ± 9 min. The remaining 70% of mitoses in *hCDC4*$^{-/-}$ cells lasted 58 ± 2.5 min, similar to those observed in parental cells, and were executed in a morphologically normal manner. No other obvious differences in cell-cycle execution were observed.

To determine whether this marked phenotype was reproducible, we disrupted the *hCDC4* gene in DLD-1, another karyotypically stable colorectal cancer cell line. We obtained a clone in which both alleles were disrupted (Fig. 2b, c), and the phenotype of this clone was indistinguishable from that of HCT116 *hCDC4*$^{-/-}$ cells. In particular, there were no obvious growth defects in *hCDC4*$^{-/-}$ cells, but there was a significant increase in cyclin E protein (Fig. 2d) and a higher percentage of micronuclei formation as compared with parental cells (22.0% versus 0.9%, $P < 10^{-5}$, $n > 400$ cells for each; Supplementary Table 2).

We examined whether the *hCDC4*$^{-/-}$ cells had acquired chromosomal instability by carrying out multicolour FISH with centromeric probes for chromosomes 7, 17, 18 and X on interphase nuclei once cells had gone through 25 generations after clone isolation. Deviations from the normal number of chromosomes were frequently observed in *hCDC4*$^{-/-}$ cells derived from either HCT116 or DLD-1, but not in their *hCDC4*$^{+/-}$ heterozygous or wild-type parental counterparts (Table 1). The degree of instability in the *hCDC4*$^{-/-}$ cells is similar to that observed in chromosomally unstable colorectal cancer cells[16]. Notably, the abnormal chromosome numbers were most commonly observed in cells that possessed micronuclei or that showed other abnormal nuclear morphology (Fig. 3a, b, d).

It was possible that the chromosomal instability phenotype observed in the two *hCDC4*$^{-/-}$ cancer lines was caused by mutations in other genes in the parental lines used to generate the knockouts lines. To investigate the effects of *hCDC4* inactivation alone, we used transient transfection of short interfering RNA (siRNA) duplexes to suppress specifically the expression of *hCDC4*

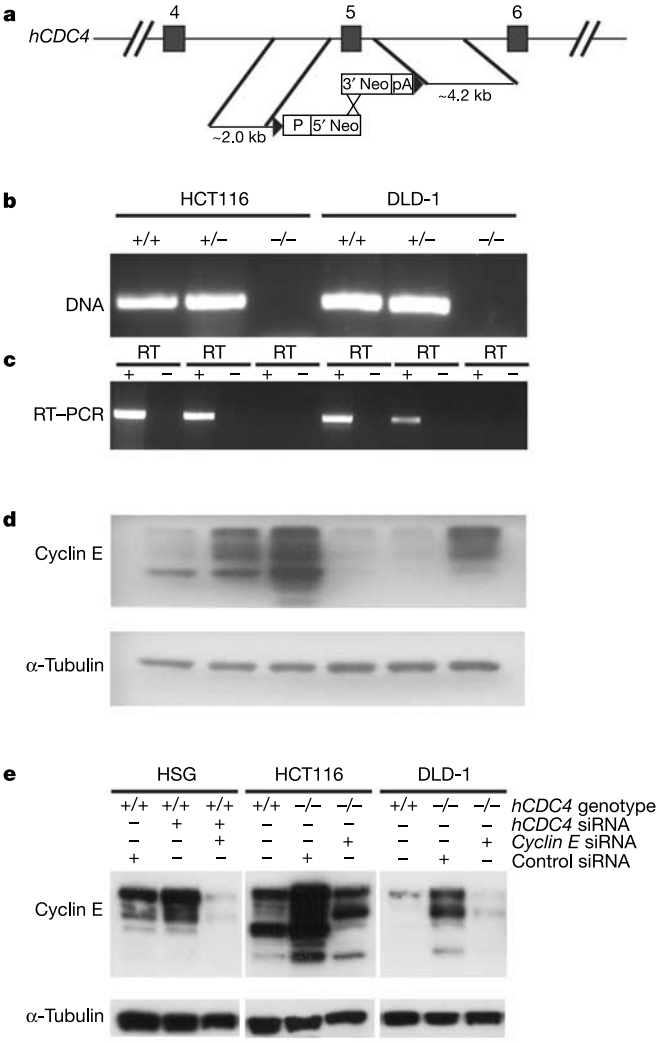

Figure 2 Disruption of *hCDC4* and *cyclin E*. **a–d**, Knockout of *hCDC4* by homologous recombination. **a**, Exon 5 was targeted for deletion by homologous recombination using 5′ and 3′ arms in a bipartite vector system. **b**, Confirmation of knockouts by a PCR screen of genomic DNA. **c**, Reverse-transcription PCR screen of cDNA. **d**, Western blotting with an antibody against cyclin E. **e**, siRNA targeting of *hCDC4* and/or *cyclin E*. The effects of targeting were assessed by western blotting with an antibody against cyclin E. Control siRNA indicates mock transfection in HSG and HCT116 *hCDC4*$^{-/-}$ cells and transfection with Lamin A/C siRNA in DLD-1 *hCDC4*$^{-/-}$ cells.

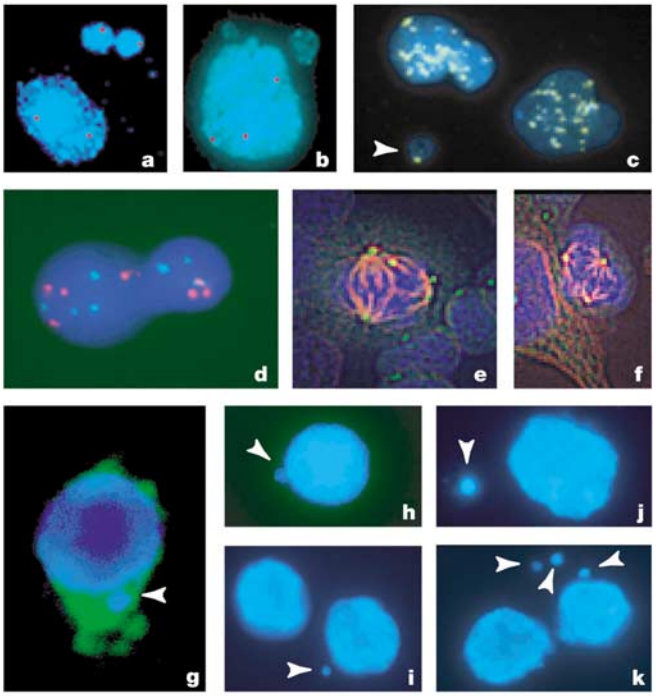

Figure 3 *hCDC4*-deficient human cells are chromosomally unstable. **a**, **b**, *hCDC4*$^{-/-}$ HCT116 cells hybridized with a chromosome-17-centromere-specific FISH probe (red dots) and counterstained for DNA content with DAPI. **c**, *hCDC4*$^{-/-}$ cells hybridized with a pan-centromeric FISH probe (green), showing centromeric DNA in a micronucleus (arrowhead). **d**, *hCDC4*$^{-/-}$ DLD-1 cells hybridized with FISH probes specific for centromeres of chromosome 7 (red) and 18 (green). **e**, **f**, Spindle dysfunction in *hCDC4*$^{-/-}$ HCT116 cells. Cells were stained with antibodies to α-tubulin (red) and γ-tubulin (green) to detect mitotic spindles and centrosomes, respectively. **g**, Cyclin E immunofluorescence (green) and DAPI counterstaining (blue) of a DLD-1 cell expressing exogenous cyclin E, showing a micronucleus (arrowhead). **h–k**, Micronuclei (arrowheads) are found in HSG cells either transfected with siRNA targeted towards *hCDC4* (**h**, **i**), or overexpressing exogenous cyclin E (**j**, **k**).

in cells derived from normal human salivary gland epithelium (HSG). A 40% decrease in *hCDC4* messenger RNA (data not shown) was sufficient to produce an increased abundance of cyclin E protein (Fig. 2e). These *hCDC4* 'knockdown' cells also showed a significant increase in the percentage of micronucleus formation (9.0% versus 3.8%, $P < 0.0001$, $n = 1{,}000$ cells for each; Fig. 3h, i, and Supplementary Table 2). It should be noted that the assessment of micronuclei as a proxy for chromosomal instability suffers from some theoretical disadvantages, but these are more problematic in long-term experiments than in the experiments described here[17].

Cyclin E is the only known target of the ubiquitin ligase activity of hCDC4. To determine whether the increased abundance of cyclin E was sufficient to reproduce the phenotype observed on inactivation of *hCDC4*, we overexpressed cyclin E in DLD-1 and HSG cells through transient transfection. An increase in the percentage of micronuclei formation (Fig. 3j, k) was observed in both types of cells as compared with cells transfected with a control expression vector (9.3% versus 3.0% for DLD-1 and 9.7% versus 3.6% for HSG, $P < 0.0001$, $n > 400$ cells for each; Supplementary Table 2). We also carried out immunofluorescence in DLD-1 cells transfected with a cyclin E expression vector, and counted micronuclei in cells staining brightly for cyclin E (Fig. 3g). We found that cells expressing large quantities of cyclin E produced significantly more micronuclei than did cells without cyclin E staining (21% versus 6%, $P < 0.001$, $n > 100$ cells for each; Supplementary Table 2).

Having shown that overexpression of cyclin E could recapitulate the micronucleus phenotype observed in cells with inactivated or suppressed *hCDC4*, we next determined whether cyclin E was necessary to produce this phenotype. Knockdown of *cyclin E* expression in the cancer lines in which *hCDC4* was knocked out significantly reduced the percentage of micronuclei formation (7.9% versus 17.5% for HCT116, and 8.5% versus 15.2% for DLD-1, $P < 0.0001$, $n = 1{,}000$ cells for each; Fig. 2e and Supplementary Table 2). Similar results were observed in HSG cells: when co-transfected with siRNA duplexes targeting both *hCDC4* and *cyclin E*, the percentage of micronucleus formation was much less than that observed when only *hCDC4* expression was knocked down (2.7% versus 9%, $P < 0.0001$, $n = 1{,}000$ cells for each; Supplementary Table 2). Taken together, these results imply that an upregulation of cyclin E is essential for the chromosomal instability phenotype observed after inactivation of *hCDC4*.

Table 1 **Measurement of chromosomal instability by FISH**

Cell line	Chromosome	Signals (%)					
		0	1	2	3	4	5
HCT116 parental	7		1	99			
	17		2	98			
	X		99	1			
HCT116 *hCDC4*$^{+/-}$	7		1.5	97	1	0.5	
	17		1.5	98		0.5	
	X	0.5	98.5	1			
HCT116 *hCDC4*$^{-/-}$	7		5.5	88	5	1	0.5
	17	1	7	88	2	2	
	X	1.5	89	9.5			
DLD-1 parental	7			98		2	
	17		2	97		1	
	18		3	93	2	2	
	X		98	2			
DLD-1 *hCDC4*$^{+/-}$	7			99		1	
	17		4	95		1	
	18		3	95	1	1	
	X		98	2			
DLD-1 *hCDC4*$^{-/-}$	7	2	4	88	4	2	
	17		14	83	2	1	
	18	2	3	89	4	2	
	X	5	86	5		4	

A total of 200 nuclei were examined for FISH signals from each of the indicated centromeric probes. $P < 10^{-7}$ for the percentage of signals off the mode in *hCDC4*$^{-/-}$ cells as compared with HCT116 wild-type or DLD-1 wild-type (*hCDC4*$^{+/+}$) cells.

Disparate cellular events and pathways have been proposed to have a role in the genetic instability found in cancer cells[18]. Only a few cancers have been shown to contain specific mutations that can promote aneuploidy[19], and the stage at which chromosomal instability occurs in tumorigenesis remains controversial[20–26]. Our results suggest that mutational inactivation of *hCDC4* is likely to be a chief cause of chromosomal instability in cancers and that this mutation can occur at an early stage. These data lend support to the hypothesis that the chromosomal instability of cancer cells, like their abnormal growth control, is a direct result of specific genetic alterations. □

Methods

Sequencing

Primers for PCR amplification and direct sequencing of exons 2–10 of *hCDC4* were designed with the NetPrimer program (Premier Biosoft) and synthesized by GeneLink. PCR amplification and sequencing were done on tumour DNA from 58 adenomas and 190 early passage colorectal cancer cell lines passaged as xenografts in nude mice or *in vitro* as described[27]. Sequencing was done by using 384-capillary automated sequencing apparatus (SpectruMedix). We confirmed that all mutations were somatic by amplifying and sequencing patient-matched normal DNA. Sequence traces were analysed with the Mutation Explorer software package (SoftGenetics).

Knockout and siRNA

General methods for gene disruption in colorectal cancer cells using a bipartite vector system have been described[14]. Constructs and primer sequences are available from the authors on request.

The coding strand of the RNA oligonucleotide duplex directed to *hCDC4* was 5′-GAGUUGGCACUCUAUGUGC-3′ and had 3′ dTdT overhangs (Dharmacon). We purchased siRNA duplexes for Lamin A/C from Dharmacon. siRNA duplexes targeting cyclin E were constructed by using a Shortcut RNAi kit (NEB) in accordance with the manufacturer's protocols. Primer sequences are available from the authors on request. We obtained HSG cells[28] from A. Rosen and grew them in DMEM medium supplemented with 10% fetal bovine serum. RNA duplexes were transfected into cells by using Oligofectamine (Invitrogen) in accordance with the manufacturer's instructions. Cellular protein, mRNA and nuclear structure were assayed 72 h after transfection. We determined mRNA levels by real-time PCR and evaluated nuclear structure after staining with 4′,6-diamidino-2-phenylindole dihydrochloride (DAPI).

Protein expression and immunoprecipitation

For overexpression of cyclin E, the cyclin E open reading frame was cloned into pBI-EGFP[19] and transiently transfected into DLD-1 cells (American Type Culture Collection) by using Lipofectamine (Invitrogen). For immunoprecipitation, a fragment of *hCDC4* complementary DNA, nucleotides 374 to 1,874, was amplified from DLD-1 cDNA and cloned in-frame into the pCMV-Myc (Clontech) multiple-cloning site using the *Bgl*II and *Not*I restriction sites. The Arg465Cys mutation was introduced by sexual PCR and cloned into the vector in a similar way. Primer sequences are available from the authors on request.

Cyclin E full-length cDNA was cloned into pIRES-Hyg2 (Clontech). Cloned constructs were co-transfected into DLD-1 cells with Lipofectamine (Invitrogen) at a 1:3 or 1:10 (mass:mass) ratio of Myc–hCDC4:cyclin E. Crude extracts were collected after 24 h by lysing cells in ice-cold buffer containing 50 mM Tris, 0.5% deoxycholate, 1% Nonidet P-40, 150 mM NaCl and Complete protease inhibitors (Roche) and subsequently incubated with agarose beads conjugated to mouse monoclonal antibody directed towards the c-Myc epitope tag (9E10, Santa Cruz Biotech).

Immunoblotting

Protein extracts from HCT116, DLD-1 and derivative lines were prepared by lysing cells on ice in RIPA buffer (Boston BioProducts). We briefly sonicated the extracts and removed debris by centrifugation at 10,000*g* for 15 min at 4 °C. Immunoblotting was done by using Immobilon P membranes (MilliPore) according to the manufacturer's instructions. Commercially available antibodies to cyclin E (Santa Cruz Biotech) and c-Myc (Roche) were used as recommended by the manufacturer. Signals were developed using the ECL Advance western blot detection kit (Amersham).

Immunofluorescence

For α-tubulin and γ-tubulin staining, cells grown on chamber slides were fixed in 4% paraformaldehyde for 10 min. After permeabilization in 0.1% Triton X-100, cells were blocked in a solution of 4% goat serum in PBS, and then incubated with monoclonal antibodies to α-tubulin (IgG2a) and γ-tubulin (IgG1), followed by isotype-specific antibodies coupled to Alexa 594 and Alexa 488 (Molecular Probes). Images were acquired and deconvoluted by the MetaMorph software package (Molecular Devices). For cyclin E staining, cells grown on slides were fixed in ice-cold methanol for 10 min. Cells were blocked with 10% goat serum in PBS, and incubated first with monoclonal antibodies to cyclin E (HE111, Santa Cruz Biotech) and then with a fluorescein isothiocyanate (FITC)-conjugated secondary antibody against mouse IgM and IgG (Pierce). Fixed slides were stained with DAPI by using traditional methods.

Time-lapse imaging

Cells were stably transfected with pBOS–histone-H2B–GFP[15] and analysed on a TE200 inverted microscope (Nikon) with a ×40 objective enclosed in a temperature- and carbon-dioxide-controlled incubator (Neve). Images were acquired with a CCD camera (Princeton) at intervals ranging from 1 to 10 min and analysed by the MetaMorph software program (Molecular Devices).

Fluorescent *in situ* hybridization

Methods for FISH analysis with chromosome-specific centromeric probes and quantitative analysis of chromosome loss rates have been described[16]. A pan-centromeric FISH probe (IDbright Pan-Centromeric, ID Labs) was used in accordance with the manufacturer's instructions. Multicolour FISH with centromeric probes for chromosomes 7, 17, 18 and X was also done on interphase nuclei once cells had gone through 25 generations after clone isolation. To prepare metaphase spreads, we treated cells with 0.1 $\mu g\,ml^{-1}$ colcemid (KaryoMax, Invitrogen) for 1 h and processed them by standard methods. Karyotyping was done by standard G-banding procedures.

Received 17 September 2003; accepted 5 January 2004; doi:10.1038/nature02313.

1. Boveri, T. *Zur Frage der Enstehung maligner Tumoren* (Gustav Fischer, Jena, Germany, 1914).
2. Winston, J. T., Koepp, D. M., Zhu, C., Elledge, S. J. & Harper, J. W. A family of mammalian F-box proteins. *Curr. Biol.* **9,** 1180–1182 (1999).
3. Schwab, M. & Tyers, M. Cell cycle. Archipelago of destruction. *Nature* **413,** 268–269 (2001).
4. Bartek, J. & Lukas, J. Cell cycle. Order from destruction. *Science* **294,** 66–67 (2001).
5. Moberg, K. H., Bell, D. W., Wahrer, D. C., Haber, D. A. & Hariharan, I. K. Archipelago regulates Cyclin E levels in *Drosophila* and is mutated in human cancer cell lines. *Nature* **413,** 311–316 (2001).
6. Spruck, C. H. *et al. hCDC4* gene mutations in endometrial cancer. *Cancer Res.* **62,** 4535–4539 (2002).
7. Strohmaier, H. *et al.* Human F-box protein hCdc4 targets cyclin E for proteolysis and is mutated in a breast cancer cell line. *Nature* **413,** 316–322 (2001).
8. Orlicky, S., Tang, X., Willems, A., Tyers, M. & Sicheri, F. Structural basis for phosphodependent substrate selection and orientation by the SCF_{Cdc4} ubiquitin ligase. *Cell* **112,** 243–256 (2003).
9. Guex, N. & Peitsch, M. C. SWISS-MODEL and the Swiss-PdbViewer: an environment for comparative protein modeling. *Electrophoresis* **18,** 2714–2723 (1997).
10. Koepp, D. M. *et al.* Phosphorylation-dependent ubiquitination of cyclin E by the SCF^{Fbw7} ubiquitin ligase. *Science* **294,** 173–177 (2001).
11. Spruck, C. H., Won, K. A. & Reed, S. I. Deregulated cyclin E induces chromosome instability. *Nature* **401,** 297–300 (1999).
12. Nash, P. *et al.* Multisite phosphorylation of a CDK inhibitor sets a threshold for the onset of DNA replication. *Nature* **414,** 514–521 (2001).
13. Goh, P. Y. & Surana, U. Cdc4, a protein required for the onset of S phase, serves an essential function during G_2/M transition in *Saccharomyces cerevisiae*. *Mol. Cell. Biol.* **19,** 5512–5522 (1999).
14. Jallepalli, P. V. *et al.* Securin is required for chromosomal stability in human cells. *Cell* **105,** 445–457 (2001).
15. Kanda, T., Sullivan, K. F. & Wahl, G. M. Histone–GFP fusion protein enables sensitive analysis of chromosome dynamics in living mammalian cells. *Curr. Biol.* **8,** 377–385 (1998).
16. Lengauer, C., Kinzler, K. W. & Vogelstein, B. Genetic instability in colorectal cancers. *Nature* **386,** 623–627 (1997).
17. Savage, J. R. Acentric chromosomal fragments and micronuclei: the time-displacement factor. *Mutat. Res.* **225,** 171–173 (1989).
18. Lengauer, C., Kinzler, K. W. & Vogelstein, B. Genetic instabilities in human cancers. *Nature* **396,** 643–649 (1998).
19. Cahill, D. P. *et al.* Mutations of mitotic checkpoint genes in human cancers. *Nature* **392,** 300–303 (1998).
20. Thiagalingam, S. Evaluation of chromosome 18q in colorectal cancers. *Nature Genet.* **13,** 343–346 (1996).
21. Pihan, G. A. *et al.* Centrosome defects and genetic instability in malignant tumors. *Cancer Res.* **58,** 3974–3985 (1998).
22. Rajagopalan, H., Nowak, M. A., Vogelstein, B. & Lengauer, C. The significance of unstable chromosomes in colorectal cancer. *Nature Rev. Cancer* **3,** 695–701 (2003).
23. Sieber, O. M., Heinimann, K. & Tomlinson, I. P. Genomic instability—the engine of tumorigenesis? *Nature Rev. Cancer* **3,** 701–708 (2003).
24. Nowak, M. A. *et al.* The role of chromosomal instability in tumor initiation. *Proc. Natl Acad. Sci. USA* **99,** 16226–16231 (2002).
25. Sieber, O. M. *et al.* Analysis of chromosomal instability in human colorectal adenomas with two mutational hits at APC. *Proc. Natl Acad. Sci. USA* **99,** 16910–16915 (2002).
26. Shih, I. M. *et al.* Evidence that genetic instability occurs at an early stage of colorectal tumorigenesis. *Cancer Res.* **61,** 818–822 (2001).
27. Bardelli, A. *et al.* Mutational analysis of the tyrosine kinome in colorectal cancers. *Science* **300,** 949 (2003).
28. Shirasuna, K., Sato, M. & Miyazaki, T. A neoplastic epithelial duct cell line established from an irradiated human salivary gland. *Cancer* **48,** 745–752 (1981).

Supplementary Information accompanies the paper on **www.nature.com/nature.**

Acknowledgements We thank L. Meszler and L. Morsberger for technical assistance; A. Rosen and S. White for reagents; and the members of our Center for Cancer Genetics and Therapeutics for help and support. This work was supported by the Clayton Fund, NIH grants, and a Translational Research Award from the Virginia and D. K. Ludwig Fund for Cancer Research.

Competing interests statement The authors declare that they have no competing financial interests.

Correspondence and requests for materials should be addressed to C.L. (lengauer@jhmi.edu).

Spatially restricted microRNA directs leaf polarity through ARGONAUTE1

Catherine A. Kidner & Robert A. Martienssen

Cold Spring Harbor Laboratory, Cold Spring Harbor, New York 11724, USA

Gene regulation by RNA interference requires the functions of the PAZ domain protein Argonaute. In plants, mutations in *ARGONAUTE1* (*AGO1*) are associated with distinctive developmental defects that suggest a role for microRNA (miRNA) in organ polarity. Potential targets of miRNA regulation are the homeodomain/leucine zipper genes *PHABULOSA* (*PHB*) and *PHAVOLUTA* (*PHV*)[1]. These genes are expressed in a polar fashion in leaf primordia and are required for adaxial cell fate[2,3]. Here we show that a 21-nucleotide miRNA that directs cleavage of *PHB*/*PHV* messenger RNA accumulates first in the embryonic meristem, and then in the abaxial domain of the developing leaf. miRNA distribution is disrupted by mutations in AGO1, indicating that AGO1 affects the regulation of miRNA. In addition, interactions between homeodomain/leucine zipper genes and an allelic series of *ago1* indicate that miRNA acts as a signal to specify leaf polarity.

Surgical isolation of early leaf primordia results in outgrowth of 'centric' or radial organs, suggesting that a meristem-derived signal directs adjacent regions of the leaf primordia to adopt an adaxial fate, and directs the regions of the leaf primordia furthest from the meristem to become abaxial[4]. In *Arabidopsis*, mutants in *AGO1* (ref. 5) and the related gene *PINHEAD*/*ZWILLE* (*PNH*/*ZLL*)[6,7] have overlapping defects in meristem maintenance and leaf polarity consistent with a defect in this signalling process, and the two genes are partially redundant[6]. However, whereas *ago1* leaves are adaxialized (see below), *pnh* leaves are weakly abaxialized[6].

Argonaute genes are defined by carboxy-terminal PAZ and PIWI domains, and are widespread in eukaryotes[8]. In *Drosophila*, mutations in *sting*/*aubergine* and *dAGO1* have defects in germline development[9], and Sting/Aubergine is required for translation of *oskar* in the polar granules[10]. Argonaute genes are required for post-transcriptional gene silencing and RNA interference (RNAi)[8,11], and AGO1-like proteins are part of the RISC (RNA interference silencing complex), which targets mRNA for degradation using miRNA as a guide[12,13]. miRNAs from *Arabidopsis* match several transcription factor genes, potentially accounting for *ago1* and *pnh/zll* phenotypes[1,14].

We isolated an allelic series of *AGO1* to investigate its role in polarity (Fig. 1). The strong alleles *ago1-9* and *ago1-10* are frame-shift truncations of 384 and 404 amino acids respectively, deleting the PAZ and PIWI domains. Vegetative organs are strap-like or radial[5,6], with radial organs (*ago1-10*) or reduced flowers (*ago1-9*) in the inflorescence (Fig. 1), suggesting a complete loss of adaxial/abaxial polarity. Ectopic ovules are found occasionally (*ago1-9*) or frequently (*ago1-11* and *ago1-12*) on the outside (abaxial) carpel wall, usually near the base (Fig. 1c). *ago1-11* and *ago1-12* are both weak alleles that retain the PAZ domain. *ago1-11* has an A-to-T conversion at the splice acceptor site of the fourteenth intron, leading to mis-splicing and exon skipping. The first pair of leaves are sometimes radial or trumpet-shaped but the remainder are flattened. Trichomes appear on the abaxial rather than the adaxial side of early leaves, suggesting an inversion of epidermal polarity in this weak allele (Fig. 1d). *ago1-12* has a C-to-T transition at nucleotide 2,414, resulting in a leucine substitution for an absolutely conserved histidine residue in the PIWI domain. *ago1-12* leaves are almost always trumpet-shaped with glossy dark-green tissue (adaxial) outside and reflective epidermis (abaxial) inside the